Aquatic Toxicology 187 (2017) 18–28

Contents lists available at ScienceDirect

Aquatic Toxicology

journal homepage: www.elsevier.com/locate/aquatox

Research Paper

Interaction between the zebrafish (*Danio rerio*) organic cation transporter 1 (Oct1) and endo- and xenobiotics

Ivan Mihaljević[a], Marta Popović[a,b], Roko Žaja[a], Nikola Maraković[c], Goran Šinko[c], Tvrtko Smital[a,*]

[a] *Laboratory for Molecular Ecotoxicology, Division for Marine and Environmental Research, Ruđer Bošković Institute, Bijenička cesta 54, 10000, Zagreb, Croatia*
[b] *Department of Oncology, University of Oxford, Old Road Campus Research Building, Roosevelt Drive, Oxford, United Kingdom*
[c] *Biochemistry and Organic Analytical Chemistry Unit, Institute for Medical Research and Occupational Health, Ksaverska cesta 2, 1000 Zagreb, Croatia*

ARTICLE INFO

Article history:
Received 29 November 2016
Received in revised form 9 February 2017
Accepted 15 March 2017
Available online 18 March 2017

Keywords:
Organic cation transporter 1 (Oct1)
Zebrafish
Functional characterization
Transient and stable transfection
Novel fluorescent substrates
Interaction with xenobiotics

ABSTRACT

Organic cation transporters (OCTs) serve as uptake transporters of numerous endo- and xenobiotics. They have been in the focus of medical toxicological research for more than a decade due to their key role in absorption, distribution, metabolism and excretion due to their expression on basolateral membranes of various barrier tissues. OCTs belong to the SLC22A family within the SLC (Solute carrier) protein superfamily, with three co-orthologs identified in humans (OCT1, 2 and 3), and two Oct orthologs in zebrafish (Oct1 and Oct2). The structural and functional properties of zebrafish Octs, along with their toxicological relevance, have still not been explored. In this study, we performed a functional characterization of zebrafish Oct1 using transient and stable heterologous expression systems and model fluorescent substrates as the basis for interaction studies with a wide range of endo- and xenobiotics. We also conducted a basic topology analysis and homology modeling to determine the structure and membrane localization of Oct1. Finally, we performed an MTT assay to evaluate the toxic effects of the seven interactors identified – oxaliplatin, cisplatin, berberine, MPP^+, prazosin, paraquat and mitoxantrone – in human embryonic kidney cells (HEK293T) stably expressing zebrafish Oct1 (HEK293T-drOct1 cells). Our results show that the zebrafish Oct1 structure consists of 12 transmembrane alpha helices, which form the active region with more than one active site. Five new fluorescent substrates of Oct1 were identified: ASP+ (K_m = 26 μM), rhodamine 123 (K_m = 103.7 nM), berberine (K_m = 3.96 μM), DAPI (K_m = 780 nM), and ethidium bromide (K_m = 97 nM). Interaction studies revealed numerous interactors that inhibited the Oct1-dependent uptake of fluorescent substrates. The identified interactors ranged from physiological compounds (mainly steroid hormones) to different classes of xenobiotics, with IC_{50} values in nanomolar (e.g., pyrimethamine and prazosin) to millimolar range (e.g., cimetidine). Cytotoxicity experiments with HEK293T-drOct1 cells enabled us to identify berberine, oxaliplatin and MPP+ as substrates of Oct1. The data presented in this study provide the first insights into the functional properties of zebrafish Oct1 and offer an important basis for more detailed molecular and ecotoxicological characterizations of this transporter.

1. Introduction

Organic cation transporters (OCTs in humans; Octs in other taxa) are members of the SLC22 (Solute Carrier) family responsible for the uptake of numerous organic cations across the plasma membrane. Phylogenetically, organic cation and organic cation/carnitine transporters form the largest clade of Octs, and together with organic anion transporter (Oat) clade they make up the SLC22 family. OCTs/Octs are highly conserved genes within vertebrate phyla, whose ancestry extends all the way to lamprey and sharks (Zhu et al., 2015). They are represented with three co-orthologs in rep-

Abbreviations: ADME, absorption, distribution, metabolism and excretion; ASP+, 4-(4-(dimethylamino)styryl)-*N*-methylpyridinium iodide; DAPI, 4′,6-diamidino-2-phenylindole; DBT, dibutyltin chloride; DMEM, Dulbecco's modified eagle's medium; HEK239, human embryonic kidney cell line; MPP+, 1-methyl-4-phenylpyridinium; MTT, 3-(4,5-dimethylthiazol-2-yl)-2,5-diphenyltetrazolium bromide; OCTs, organic cation transporters; TBA, tetrabutylammonium; TBT, tributyltin chloride; TEA, tetraethylammonium; TKIs, tyrosine kinase inhibitors; TMDs, transmembrane domains; TPenA, tetrapentylammonium.

* Corresponding author.
E-mail address: smital@irb.hr (T. Smital).

http://dx.doi.org/10.1016/j.aquatox.2017.03.012
0166-445X/

tiles, birds and humans, while in teleost fish and amphibians Octs have two and one ortholog(s), respectively (Mihaljevic et al., 2016). Mammalian OCT1-3/Oct1-3 are expressed in a number of toxicologically important tissues essential for metabolization and/or excretion of endo- and xenobiotics, especially liver and kidneys. When comparing the tissue expression of human OCTs, OCT1 is highly expressed in the liver, in sinusoidal hepatocyte membranes (Gorboulev et al., 1997), and is also found in epithelial cells and neurons (Koepsell et al., 2003). OCT2 is highly expressed in kidney in basolateral membranes of all three segments of the proximal tubule (Motohashi et al., 2002). It is also present in the basolateral membranes of the small intestine (Gorboulev et al., 1997), the luminal membrane of trachea and epithelial cells of bronchi (Lips et al., 2005), and the brain (Busch et al., 1996). In mice, there are also three Oct co-orthologs expressed in the entire proximal tubule, with a dominant expression of Oct1 (Schlatter et al., 2014). Mouse Oct1 is also expressed in the basolateral membranes of enterocytes (Chen et al., 2001). Oct2 expression in rat brain showed localization in the apical membrane of the choroid plexus epithelial cells (Sweet et al., 2001). Human OCT3 has a ubiquitous expression pattern. Contrary to OCT1 and OCT2, it is weakly expressed in the epithelial cells of toxicologically relevant tissues and neurons, but is present in muscle and glia cells (Inazu et al., 2003; Zhang et al., 2008).

Human OCTs are highly polyspecific and transport organic cations with a one or two positive charge or weak bases with positive charge at physiological pH (Nies et al., 2011). Despite the common electrogenic nature of OCT-mediated transport, the driving forces of the transport mechanism differ between members, with positive charge and molecular volume as the major drivers of OCT1-mediated transport, and positive charge and H-bonding properties as drivers of OCT2 transport (Hendrickx et al., 2013). OCT1 and 2 share overlapping substrate specificities and occasionally similar substrate affinities (Nies et al., 2011). A great number of OCT inhibitors have been identified, ranging from physiologically important compounds such as steroid hormones and neurotransmitters, neuromodulators and their metabolites, to a prominent number of xenobiotic inhibitors (Nies et al., 2011; Koepsell, 2013). The number of identified OCT1 substrates is much lower compared to the number of known inhibitors, which is a consequence of the complex assay procedures used for detecting OCT1/Oct1 substrates. Hydrophobic compounds that passively cross the plasma membrane and whose transport is facilitated by OCTs are hard to identify as OCT substrates, especially if their K_m values are high, which would cause hardly noticeable differences between OCT-mediated and passive transport (Koepsell, 2015).

An additional reason for the disproportion between the low number of identified OCT-transported substrates (competitive inhibitors) and the much higher number of non-transported interactors (un- or noncompetitive inhibitors) is the complex structure of the OCT active region. OCTs/Octs consist of twelve transmembrane alpha helices (transmembrane domains, TMDs), with a large extracellular loop between the first and second TMDs, and an intracellular loop between the sixth and seventh TMD. The spatial organization of the twelve TMDs within the plasma membrane and joining loops determines the structure of the active cleft (Gorboulev et al., 2005). Eight crucial amino acid residues that define substrate affinities and the transport mechanism have been identified within the OCT1/Oct1 active region (Popp et al., 2005; Volk et al., 2009). Apart from a complex interaction of OCT substrates with the identified amino acid residues within the substrate-binding region, OCT transport activity is regulated by post-translational modifications that occur on extracellular (glycosylation) and intracellular (phosphorylation) loops, and affect the transport activity through the regulation of membrane localization and oligomerization of OCTs (Keller et al., 2011; Brast et al., 2012; Koepsell, 2015).

The described complexity of the OCTs/Octs active region can explain their polyspecific characteristics. Due to the size of the active cleft and availability of amino acid residues within the cleft, OCTs/Octs can interact with a vast number of potential substrates. This is why organic cation transporters play such an important role in the cellular uptake of diverse organic cations. Consequently, from an (eco)toxicological perspective, owing to their tissue localization in barrier tissues and function in transport of xenobiotics such as paraquat, ethidium bromide, quaternary ammonium compounds and numerous others, OCTs/Octs are highly important elements of cellular absorption, distribution, metabolism and excretion (ADME) processes (Nies et al., 2011).

The structural and functional properties of fish Octs, along with their toxicological relevance, are still poorly understood. We have previously identified two zebrafish Oct genes, *slc22a2* annotated as *oct1*, and *slc22a3* annotated as *oct2* (Mihaljevic et al., 2016). Phylogenetic and conserved synteny analysis revealed orthologous relationships between zebrafish genes – *oct1* on chromosome 20 and *oct2* on chromosome 17–and the human OCT gene cluster on chromosome 6. Zebrafish Oct1 is highly expressed in the kidneys of both sexes as well as the male liver (Mihaljevic et al., 2016). The expression profile of Oct1 is similar to its human orthologs, OCT1 and OCT2, which are expressed in the basolateral membranes of the liver and kidney. Therefore, Oct1 in zebrafish could have a defensive role similar to human orthologs. Based on our previous findings, in this study we focused on the functional characterization of zebrafish Oct1. We used transient and stable *in vitro* heterologous expression systems and model fluorescent substrates as the basis for interaction studies with a wide series of endo- and xenobiotics, followed by topology analysis and homology modeling, which enabled us to determine the structure and membrane localization of zebrafish Oct1. Finally, we performed cytotoxicity assays with Oct1 overexpressing cells to identify Oct1 substrates and evaluate the Oct1-mediated toxic effects of the identified interactors.

2. Materials and methods

2.1. Chemicals

All fluorescent dyes were purchased from Sigma-Aldrich (Taufkirchen, Germany), except for ethidium bromide which was purchased from Serva Electrophoresis GmbH (Heidelberg, Germany). All of the other chemicals were purchased from Sigma-Aldrich (Taufkirchen, Germany) or Carl Roth GmbH (Karlsruhe, Germany).

2.2. Cloning and heterologous expression

A full-length zebrafish *oct1* sequence was obtained from zebrafish cDNA by polymerase chain reaction using high fidelity Phusion DNA polymerase (Thermo Scientific, MA, USA) and specifically designed primers with NotI and HindIII restriction sites on the forward, and KpnI and XbaI restriction sites on the *oct1* reverse primers. An amplified DNA fragment was cloned into a linearized pJET 2.0 vector (Invitrogen, Carlsbad, CA). Zebrafish *oct1* sequence was verified by DNA sequencing using automated capillary electrophoresis (ABI PRISM® 3100-Avant Genetic Analyzer) at the Ruđer Bošković Institute DNA Service (Zagreb, Croatia). Sequenced genes of each clone were compared to the reported gene sequences from the NCBI and ENSEMBL databases. The verified *oct1* sequence was subcloned into the pcDNA3.1(+) and pcDNA3.1/His vectors (Invitrogen, Carlsbad, CA).

Transient transfection of human embryonic kidney cells (HEK293T) was based on the previously described procedure by Popovic et al. (2013) using polyethyleneimine (PEI) as the transfec-

tion reagent. In order to evaluate transfection efficiency, separate cells were transfected with pcDNA3.1/His/LacZ (Invitrogen, Carlsbad, CA) plasmid and transfection efficiency was evaluated 24 h after transfection with the LacZ staining protocol (Sambrook et al., 1989).

2.3. Development of the Oct1-expressing cell line

Stable expression of Oct1 in genetically engineered HEK293 Flp-In cells was achieved using targeted integration of the Oct1 sequence cloned into integration vector pcDNA5. pcDNA5/Oct1 constructs were specifically targeted into the genome of Flp-In™-293 Cell Line following the manufacturer's instructions. In short, 300 ng of the pcDNA5/Oct1 construct were co-transfected with the helper plasmid pOG44 in a 1:9 ratio (2.7 μg DNA) in the cells plated in a 6-well Plate 48 h before transfection. After 72 h, the cells were transferred to a 25 cm^2 cell culture flask and grown on Dulbecco's Modified Eagle Medium (DMEM) with 10% fetal bovine serum. After overnight cells attachment, hygromycin B was added to the final concentration of 100 mg/mL. The medium was changed every 3–4 days and hygromycin B selection continued until single colonies appeared (approximately 20 days).

2.4. Transport assays

Transfected cells that showed more than 70% of transfection efficiency were used in the subsequent transport assays. Transfection efficiency was determined using LacZ staining (data not shown). Five fluorescent compounds were tested as potential Oct1 substrates: 4-(4-(dimethylamino)styryl)-*N*-methylpyridinium iodide (ASP+), rhodamine 123 (Rh123), berberine, 4-,6-diamidino-2-phenylindole (DAPI) and ethidium bromide (EtBr). The cellular uptake of all of the substrates was measured in a sodium-based transport medium (145 mM NaCl, 3 mM KCl, 1 mM $CaCl_2$, 0.5 mM $MgCl_2$, 5 mM glucose and 10 mM Tris, pH 7.4). To obtain concentration-response curves of fluorescent substrates, 50 μL of five-time concentrated fluorescent substrates were added to the preincubation medium and incubated 5–15 min at 37 °C, depending on the substrate used. After the incubation, the cells were washed two times with 250 μL of pre-chilled transport medium and lysed with 0.1% of sodium dodecyl sulphate (SDS) for 30 min. Lysed cells were transferred to 96-well black microplates and the fluorescence was measured with a microplate reader (Infinite M200, Tecan, Salzburg, Austria). The transport rates were determined by measuring the fluorescence of Oct1-transfected cells and mock-transfected cells. The final fluorescence value was calculated by subtracting the fluorescence of mock-transfected cells from Oct1-transfected cells. To calculate and express the transport rates of fluorescent substrates as pmol of substrate per mg of protein per minute, we determined the calibration curves of the fluorescent dyes in 0.1% SDS, and in the cell matrix dissolved in the 0.1% SDS. Total protein concentration was measured using the Bradford assay (Bradford, 1976).

After determination of transport kinetics for fluorescent dyes, ASP+ and Rh123 were used in subsequent inhibition assays. Inhibition measurements were based on the co-exposure of transfected cells and mock control with the determined model substrate and potential interactor. The cells were preincubated for 10 min in transport medium, then for 40 s with the test compounds, followed by 5 and 10 min of incubation with ASP+ and Rh123, respectively. The concentrations of the model substrates used were in the linear part of the previously determined concentration-response curves. The interaction screens were performed with one or two concentrations of the tested compounds, and for the interactors that showed an uptake inhibition above 50%, IC_{50} values were determined. Compounds with IC_{50} values in nanomolar and low micromolar range (<5 μM) were considered very strong interactors; compounds with an IC_{50} of 5–20 μM were designated as strong interactors; compounds with determined IC_{50} values of 20–100 μM were classified as moderate interactors; and those with an IC_{50} above 100 μM were classified as weak interactors.

2.5. Western blotting and immunofluorescence

Cells from 2 wells of a 6-well microplate were collected 24 h after transfection and lysed in RIPA buffer (NaCl 150 mM, EDTA 1 mM, Tris 25 mM, NP-40 0.8%) with an AEBSF protease inhibitor cocktail (Sigma-Aldrich, Taufkirchen, Germany) for 30 min on ice. After the lysis, cells were subjected to 3 freeze/thaw cycles, briefly sonicated and centrifuged at 1000 × *g* for 10 min at 4 °C. Protein concentration in total cell lysate (TCL) was measured using the Bradford assay. Proteins (10 μg per lane) were separated by electrophoresis in 10% polyacrylamide gel with 0.1% SDS. The separated proteins were transferred to the polyvinylidene difluoride membrane (Millipore, MA, US) by semidry blotting. Blocking was performed in blocking solution (5% low fat milk, 50 mM Tris, 150 mM NaCl and 0.05% Tween 20) for 1 h. Subsequently, the membranes were washed and incubated for 2 h with anti-His antibody (1:5000) and for 1 h with goat anti-mouse IgG-HRP (1:5000) (Bio-Rad Laboratories, CA, USA) as the secondary antibody. The proteins were visualized by chemiluminescence (Abcam, Cambridge, UK) and protein size was estimated by protein marker (ThermoFischer Scientific, MA, USA). For immunofluorescence localization of proteins transiently overexpressed in HEK293T cells in 24-well culture plates on glass coverslips, cell fixation was performed with 4% paraformaldehyde in phosphate-buffered saline (PBS) for 30 min. Cells were washed three times in 100 mM glycine/PBS, permeabilized with methanol for 15 min and blocked in 5% low-fat milk for 30 min with gentle agitation at room temperature. Coverslips were transferred on microscope slides and incubated for 1 h at 37 °C with Na,K-ATPase anti-mouse primary antibody (Santa Cruz Biotechnology, CA, USA), diluted 1:150 in blocking solution, washed and incubated for 1 h at 37 °C with Cy3-conjugated anti-mouse IgG-HRP (Cyanine3) (1:150) (Santa Cruz Biotechnology). The washing and blocking steps were repeated and coverslips incubated with anti-His antibody (1:100) in blocking solution for 1 h at 37 °C in a humidity chamber, washed and incubated with secondary FITC (fluorescein isothyocyanate) antibody (1:100) in blocking solution for 1 h at 37 °C. Nuclei were stained with DAPI for 45 min at 37 °C in 300 nM DAPI/PBS. After mounting the samples in Fluoromount medium (Sigma-Aldrich, Taufkirchen, Germany), immunofluorescence was detected using a Leica TCS SP2 AOBS confocal microscope (Leica Microsystems, Wetzlar, Germany).

2.6. Homology modeling

Homology modeling was used to predict three-dimensional structures of related human (hOCT1 and hOCT2) and zebrafish (drOct1) organic cation transporters. Accelrys Discovery Studio's Build Homology Models protocol was used to build homology models of OCTs/Oct based on the alignment of a model sequence and template structure. The Build Homology Models protocol uses the MODELER (Sali and Blundell, 1993) automodel to build homology models. To model the three-dimensional structure of OCTs/Octs, the crystal structure of the Major Facilitator Superfamily (MFS) protein lactose permease (LacY) from *E. coli* (PDB ID code 1PV6) (Abramson et al., 2003) was used as a template structure, an approach previously reported by Popp et al. (2005). Accordingly, the large loops of hOCT1 and hOCT2 were excluded from modeling since LacY lacks a corresponding structure (loop between TMDs 1 and 2) or exhibits low structural similarity (loop between TMDs 6 and 7). To build homology models of human OCT1 and OCT2,

the input sequence alignment between the model sequences of OCT1 or OCT2 and the LacY template structure was used as reported by Popp et al. (2005). For the input sequence alignment between human OCT1 and LacY, 11.8% of the amino acids were identical and 32.8% of the amino acids were similar, whereas for the input sequence alignment between hOCT2 and LacY, 9.5% of the amino acids were identical and 32.7% of the amino acids were similar. To model the three-dimensional structure of zebrafish Oct1, the obtained homology model of human OCT1 was used as the template structure. The input sequence alignment between the model sequence of zebrafish Oct1 and human OCT1 template structure was obtained, where 45.8% of the amino acids were identical and 68.2% of the amino acids were similar. The remaining parameters in the Parameters Explorer of the Build Homology Models protocol were set as follows. Cut Overhangs was set to True to cut the terminal residues of the input model sequence that were not aligned with the templates. Number of Models was set to 5 to define the number of models to create from an initial structure with Optimization Level set to Low to specify the amount of molecular dynamics with simulated annealing to perform. To build refinement models on detected loop regions, i.e., the model sequence segments of at least 5 residues length which are not aligned with the templates, Refine Loops was set to True. Build Homology Models protocol uses the DOPE (Discrete Optimized Protein Energy) (Shen and Sali, 2006) method to refine loops. Refine Loops Number of Models was set to 5 to specify the number of models to be created by loop optimization, and Refine Loops Optimization Level was set to Low to specify the number of models to be created by loop optimization. Refine Loops with Use Discrete Optimized Protein Energy (DOPE) Method was set to High Resolution. After running Build Homology Models protocol, the Best Model Structure Superimposed to Templates was chosen from the generated output models for the final three-dimensional model structure of the corresponding organic cation transporter.

2.7. Cell viability assay

For *in vitro* evaluation of the toxicological role of zebrafish Oct1, upon exposure of HEK293T-drOct1 cells to potential interactors we performed a colorimetric MTT (3-(4,5-dimethylthiazol-2-yl)-2,5-diphenyltetrazolium bromide) tetrazolium reduction assay (Mosmann, 1983) with slight modifications. We used the HEK293T-drOct1 cells, and the Flp-In HEK293 cells transfected with empty vector (mock) as control. The cells were seeded in a 48-well cell culture Plate 24 h prior to exposure. The exposition lasted for 72 h, after which we determined cell viability by MTT assay, measuring formazan production at a wavelength of 578 nm.

2.8. Data analysis

All of the assays were performed in 2–4 independent experiments run in triplicates. The data shown on the Figures represent mean ± standard errors (SE) or standard deviations (SD). All of the calculations were performed using GraphPad Prism 6 for Windows as described below. The kinetic parameters, K_m and V_{max} values were calculated using the Michaelis-Menten Eq. (1),

$$V = V_{max} \times [S]/([S] + K_m) \quad (1)$$

where V is velocity (picomoles of substrate per milligram of proteins per minute), V_{max} is maximal velocity, $[S]$ is substrate concentration and K_m is the Michaelis-Menten constant.

The uptake into vector-transfected HEK293T cells was subtracted to obtain transporter-specific uptake. For the purpose of IC_{50} calculations, data were fitted to the sigmoidal four parameters dose-response model (variable slope) using the Eq. (2):

$$V = V_{maxin} + (V_{maxax} - V_{maxin})/(1 + 10^{(\log IC50 - A)h}) \quad (2)$$

where V is response, V_{maxin} represents minimum of response, V_{maxax} represents maximum of response, h is the Hill slope parameter, IC_{50} is the concentration of inhibitor that corresponds to 50% of maximal effect and A is the concentration of the tested compound.

3. Results

3.1. Topology analysis and homology modeling

Topology analysis of zebrafish Oct1 revealed 12 transmembrane α-helices or domains (TMDs), characteristic extra- and intracellular loops, and a cytoplasmic orientation of the N- and C- terminus (Fig. 1). A large extracellular loop of 105 amino acids was located between the first and the second TMD. The following five TMDs were positioned tightly next to each other up to the large intracellular loop of 62 amino acids, located between the sixth and seventh transmembrane helix. After the intracellular loop, the remaining six TMDs were tightly packed without the extra gaps in-between. Because the crystal structures of eukaryotic OCTs/Octs were not yet available, we used the structure of the bacterial LacY (PDB 1PV6) transmembrane transporter, which belongs to the Major Facilitator Superfamily of proteins and has similar structural characteristics as SLC22/Slc22 transporters (Popp et al., 2005). Using our Oct1 model, we identified crucial amino acid residues in the active site cleft and revealed characteristic spatial organizations with tertiary structure determined by transmembrane α-helices (Fig. 1, Fig. S3). Crucial amino acid residues, which were previously confirmed to interact with substrates in the active site of mammalian orthologs, were present in the zebrafish Oct1 active site cleft. The sterically accessible amino acids within the active site cleft of zebrafish Oct1 were: Phe161, Trp219, Tyr223, Thr227, Arg440, Ile443, Phe447, Gln448, and Asp475.

3.2. Protein identification and cell localization

Overexpression of His-tagged zebrafish Oct1 in HEK293T cells was confirmed by Western blot analysis (Fig. 2). Immunofluorescence analysis showed localization of Oct1 in the cell membranes. This was confirmed by co-localization of Oct1 (green) and Na/K ATPase (red), which is used as a marker for cell membranes. As the result of co-localization, the signals of the two dyes overlapped and subsequently produced an orange signal (Fig. 2).

3.3. Functional characterization of zebrafish Oct1

We identified five fluorescent dyes that showed highly enhanced accumulation in Oct1-transfected HEK293T cells in comparison to the mock-transfected cells. Time and concentration-response assays confirmed that the tested dyes were substrates of Oct1, whose transport followed the classical Michaelis-Menten kinetics. The first confirmed fluorescent substrate was 4-(4-(dimethylamino)styryl)-*N*-methylpyridinium iodide (ASP^+) which showed saturable uptake after 5 min of accumulation. Oct1 transported ASP+ with high affinity ($K_m = 26.0 \pm 1.69$ μM) following Michaelis-Menten transport kinetics (Fig. 3, Table 1). Rhodamine 123 (Rh123) was the second verified model Oct1 fluorescent substrate. Time-dependent accumulation of Rh123 in Oct1-expressing cells showed saturation of uptake after 30 min of accumulation (Fig. S1). Oct1 transported Rh123 with very high affinity ($K_m = 104 \pm 14.9$ nM), but low V_{max} (13.0 ± 0.61 pmol/mg protein/min) (Table 1). Berberine, the third identified fluorescent

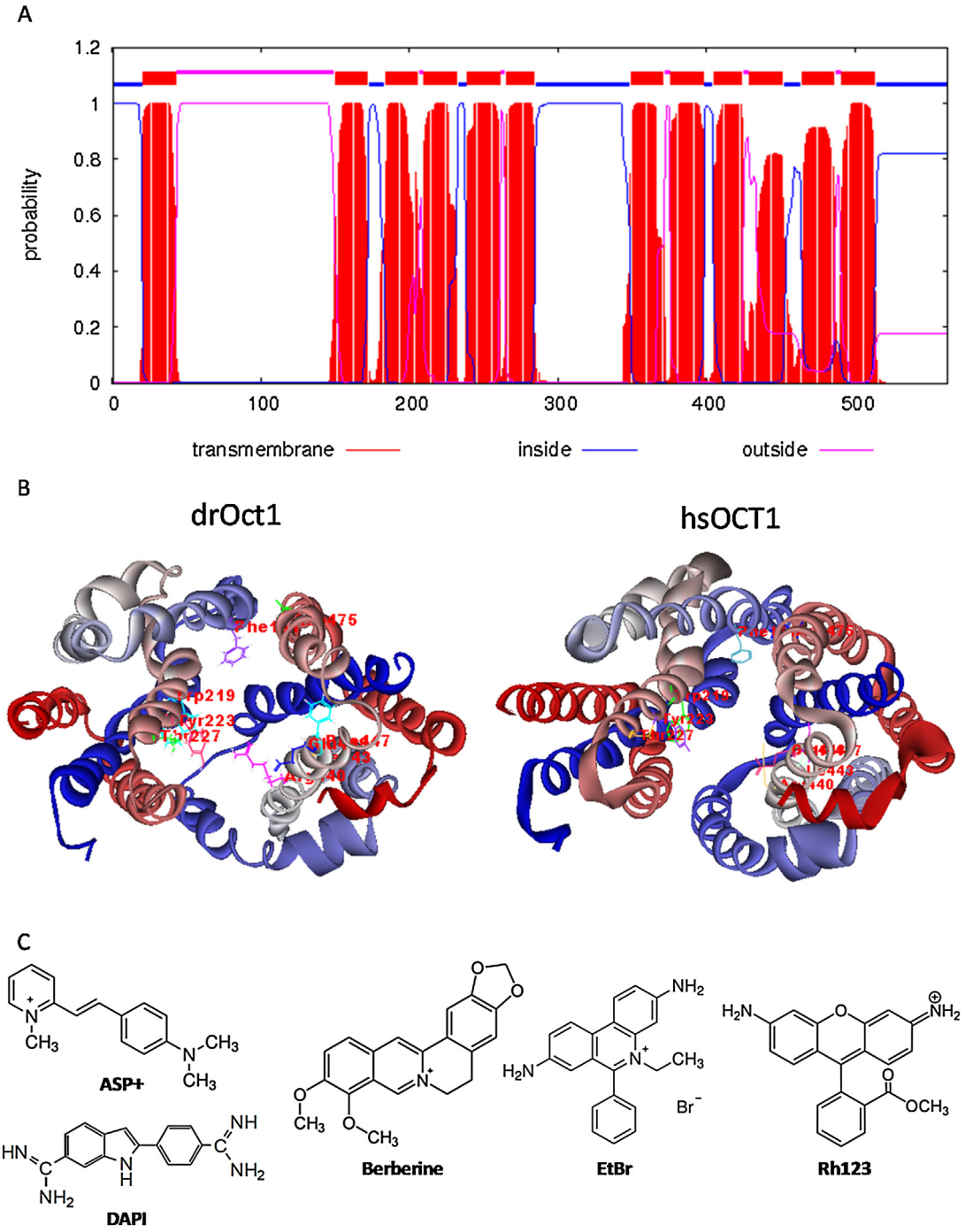

Fig. 1. (A) Graphical presentation of the zebrafish Oct1 topology analysis showing 12 transmembrane domains (TMDs) depicted in red, the large extracellular loop in pink, and the intercellular loop with N- and C- terminal ends depicted in blue. (B) Top view of predicted 3D structure of zebrafish (drOct1) and human (hsOCT1), obtained using the homology modeling. Conserved amino acid residues within the transporter active region are marked in red (Phe161, Trp219, Tyr223, Thr227, Arg440, Ile443, Phe447, Gln448, and Asp475). (C) Chemical structures of the five identified Oct1 fluorescent substrates (ASP+, Rh123, berberine, DAPI and EtBr) used for identification of accessible amino acid residues within the active site cleft. (For interpretation of the references to colour in this figure legend, the reader is referred to the web version of this article.)

substrate of Oct1, reached saturation of uptake at 30 min of accumulation (Fig. S1). Concentration-response experiments showed high affinity towards berberine (K_m = 3.96 ± 0.74 μM) (Table 1). Our further search for model Oct1 fluorescent substrates revealed DAPI as a new potential substrate. DAPI showed very fast transport with saturation of uptake at 1.5 min (Fig. S1). Concentration-response kinetics determined in real time showed high affinity of Oct1 towards DAPI (K_m = 0.78 ± 0.18 μM), but low V_{max} of 6.87 ± 0.30 pmol/mg protein/min (Table 1). Finally, similar Oct1 transport parameters were determined for ethidium bromide (EtBr) (Fig. S1). Since EtBr expresses its fluorescence maximum following interaction with DNA, we were also able to perform transport measurements in real time. Kinetic measurements revealed great difference between Oct1-transfected and mock cells, with saturation of uptake at 15 min. Zebrafish Oct1 affinity towards EtBr was very high (K_m = 96.9 ± 10.8 nM) (Table 1).

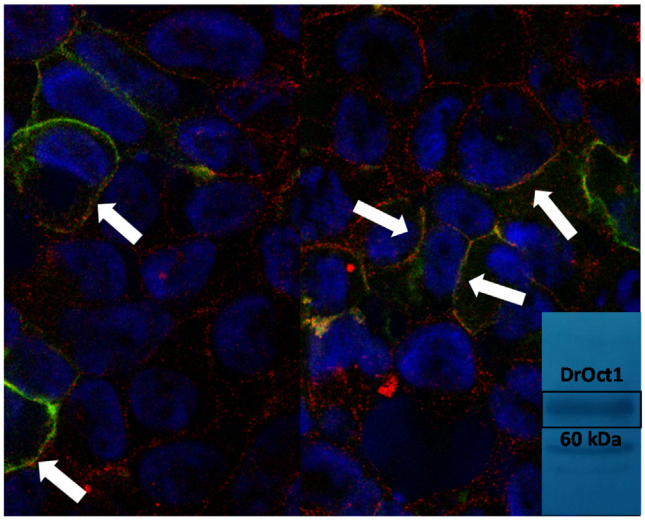

Fig. 2. Cell localization and Western blot confirmation of the zebrafish Oct1 overexpressed in HEK293T cells and tagged with the N-terminal 6xHis-tag. Immunocytochemistry was performed with fluorescein conjugated secondary antibody (FITC) that binds to the primary anti-His antibody and stains the protein in green. Nuclei are stained in blue with DAPI, and plasma membranes are stained in red after binding of primary antibody Na/K-ATPase and Cy3-conjugated IgG secondary antibody (all anti-mouse). The membrane color turns to orange (white arrows) because of the overlap of green (Oct1) and red (Na/K-ATPase). Cytosolic forms are seen as green areas in the cytoplasm. White arrows point to co-localization of Na/K-ATPase and Oct1 in cell membranes (orange). (For interpretation of the references to colour in this figure legend, the reader is referred to the web version of this article.)

Table 1
Results of the Michaelis-Menten kinetics determinations of the zebrafish Oct1-mediated uptake of five identified fluorescent substrates. Basic kinetic parameters, Km (μM) and Vmax (pmol/mg protein/min), are shown. The presented data are shown as mean of three separate experiments (n = 3) with 95% confidence interval (c.i.).

Substrate	K_m (μM)	c.i.	*Vmax* (pmol/mgprot/min)	c.i.
ASP+	26.0	22.5–29.5	993	939–1046
Rh123	0.10	0.07–0.14	13.0	11.7–14.3
Berberine	3.96	2.38–5.54	43.5	38.9–48.1
DAPI	0.78	0.39–1.17	6.87	6.22–7.52
EtBr	0.10	0.07–0.12	5.34	5.06–5.61

3.4. The interaction screening and concentration-response assays

The interaction screening assay revealed interaction of Oct1 with numerous endobiotics, confirming its polyspecific properties (Table 2, Fig. S2). Steroid hormones showed to be the most potent endogenous interactors. Our screening revealed strong interaction of zebrafish Oct1 with progesterone, a non-conjugated steroid from the group of 21-carbon progestenes (IC_{50} = 1.99 μM; Table 2). Very weak Oct1 interactions were reported with pregnenolone, the other progesten member, with only a 26.5% inhibition of ASP+ uptake. The second potent group of Oct1 steroid interactors were 19-carbon androgens, with the highest interaction determined with androstenedione (IC_{50} = 5.13 μM), testosterone (IC_{50} = 13.2 μM), and dihydrotestosterone (IC_{50} = 53.6 μM) (Table 2). The structurally similar testosterone conjugate 19-methyltestosterone showed weaker Oct1 interaction than testosterone, with an IC_{50} value of 54.1 μM (Table 2). Corticosterone, a 21-carbon glucocorticoid, showed potent Oct1 interaction with an IC_{50} value of 16.5 μM (Table 2). Another member of the glucocorticoid group, cortisol, showed weaker interaction that resulted in only a 21.9% inhibition of ASP+ uptake. One member of the 18-carbon estrogen group, β-estradiol, also showed high interaction with Oct1 yielding an IC_{50} value of 44.4 μM (Table 2). Endogenous compounds outside the group of steroid hormones that showed interaction with Oct1 were the neurotransmitter acetylcholine and the tyrosine metabolite tyramine, with IC_{50} values of 711 μM and 1002 μM, respectively (Table 2).

Table 2
IC50 values for a set of chosen endogenous and xenobiotic Oct1 interactors determined using the ASP+ (15 μM) inhibition assay. IC50 values given in μM were determined by fitting data to sigmoidal four parameter dose–response model (variable slope) in the GraphPad Prism 6. Data are given as mean of 3 separate experiments with 95% confidence intervals (c.i.).

Compound	IC_{50}	c.i.
Tripropyltin chloride	13.4	4.75–37.7
Dibutyltin chloride	0.39	0.19–0.81
Tributyltin chloride	3.90	2.56–5.96
Pyrimethamine	0.91	0.29–2.74
Prazosin	2.48	1.65–3.71
Tetraethylammonium	821	693–971
Tetrabutylammonium	28.1	11.8–66.4
Tetrapentylammonium	8.35	4.76–14.6
MPP+	22.3	8.66–57.4
Verapamil	13.7	10.6–17.8
Propranolol	119	77.7–184
Quinidine	140	111–176
Mitoxantrone	85.3	20.8–350
Cisplatine	65.7	59.3–72.8
Oxaliplatine	956	759–1204
Tamoxifen	54.3	35.2–84.0
Imipramine	62.9	41.5–95.4
Diltiazem	61.9	23.5–163
Cimetidine	522	423–645
Vandetanib	5.19	3.70–7.28
Dasatinib	23.2	13.3–43.0
Progesterone	1.99	1.53–2.58
Androstenedione	5.13	3.60–7.31
Testosterone	13.2	2.57–67.6
Dihydrotestosterone	53.6	30.6–94.0
19-methyltestosterone	54.1	36.9–79.3
Corticosterone	16.5	9.31–29.4
β-estradiol	44.4	22.2–88.7
Acetylcholine	711	465–1088
Tyramine	1002	781–1320

Apart from endogenous interactors, our screening revealed numerous xenobiotic interactors (Fig. S2). Organotin compounds, a class of well-known hazardous environmental contaminants, showed the most potent interaction with Oct1. The strongest inhibition of Oct1-mediated transport was observed with dibutyltin chloride (IC_{50} = 0.4 μM), followed by tributyltin and tripropyltin chloride with IC_{50} values of 3.9 μM and 13.4 μM, respectively (Table 2). Interaction assays revealed high affinity interactions of Oct1 with different classes of pharmaceuticals. The most potent interactions were obtained with the antimalarial drug pyrimethamine and the sympatholytic drug prazosin, with an IC_{50} of 0.91 μM and 2.48 μM, respectively (Table 2). The members of the quaternary ammonium cation family also showed high interaction levels with Oct1, especially tetrapentylammonium with a low IC_{50} of 8.35 μM, and tetrabutylammonium with an IC_{50} of 28.1 μM, whereas tetraethylammonium and tetramethylammonium showed to be less potent Oct1 interactors (Table 2). MPP^+, a model cation and known substrate of human OCT1, inhibited ASP+ uptake by zebrafish Oct1 with an IC_{50} value of 22.3 μM (Table 2). We determined strong interactions with pharmaceuticals from the family of antiarrhythmic drugs like verapamil, propranolol and quinidine, with IC_{50} values of 13.7, 119, and 139 μM, respectively. The antineoplastic drugs, mitoxantrone, tamoxifen, cisplatine and oxaliplatin inhibited Oct1-mediated ASP+ uptake with IC_{50} values of 85.3, 54.3, 65.9 and 956 μM, respectively (Table 2). We confirmed interactions of Oct1 with the antidepressant imipramine (IC_{50} = 62.9 μM), the antihypertensive drug diltiazem (IC_{50} = 61.9 μM), and the antiulcer drug cimetidine with a high IC_{50} value of 522 μM. Interaction with tyrosine kinase

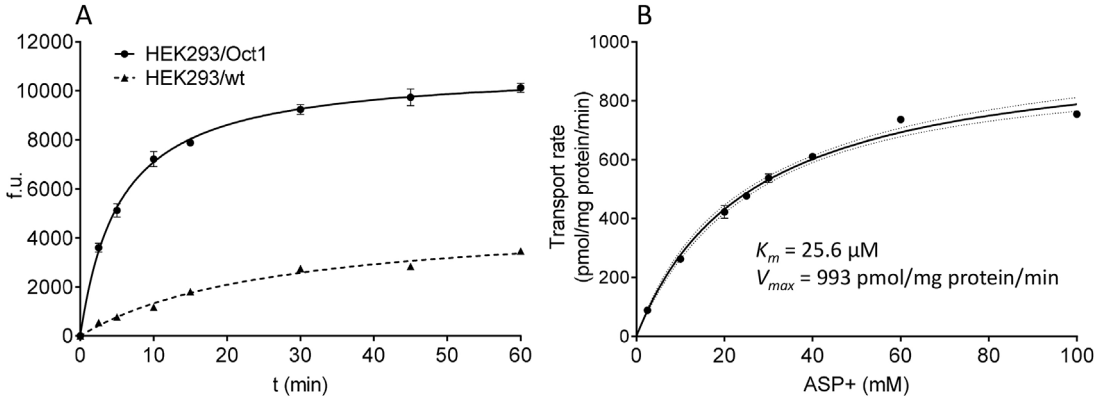

Fig. 3. Michaelis-Menten kinetics of the zebrafish Oct1-mediated uptake of fluorescent dye ASP+. A) Time dependent uptake of ASP+ by HEK293T cells overexpressing Oct1 and by mock-transfected cells, respectively. ASP+ accumulation is expressed as increase in fluorescence (fluorescence units – f.u.) over time (min). B) Concentration-response of Oct1 ASP+ uptake expressed as transport rate (pmol/mg protein/min) over ASP+ concentration (µM) after 5 min incubation with ASP+. Each data point represents the mean ± S.E. from triplicate determinations.

inhibitors was also determined. Vandetanib inhibited an ASP+ uptake with a low IC_{50} value of 3.74 µM, whereas dasatinib inhibition resulted in a higher IC_{50} of 29.1 µM (Table 2).

3.5. Modulation of toxicity using overexpression of Oct1

We were able to discriminate transported compounds (i.e., substrates) of the zebrafish Oct1 from those that were not through the exposure of stably transfected HEK293T-drOct1 cells to previously identified Oct1 interactors and observing the shift in related concentration-response curves. Oct1-overexpressing cells exposed to a competitive inhibitor were more sensitive to its toxic effect, which resulted in lower EC_{50} values in comparison with mock-transfected cells. The highest, approximately 6-fold, shift in EC_{50} values was observed with the known human OCT substrate MPP+, followed by the antineoplastic oxaliplatin and alkaloid berberine, which both caused approximately a 5-fold shift in their respective EC_{50} values (Fig. 4). The other investigated interactors such as mitoxantrone, cisplatin, paraquat and prazosin showed toxic effects with EC_{50} values of 0.85, 1.47, 1.2 and 31.39 µM, respectively. However, as there was no shift in these compounds' EC_{50} values in the transfected compared to mock-transfected cells, we concluded they were not Oct1 substrates and observed that the cytotoxic effect of these compounds may have been due to passive uptake (Fig. 5).

Once we were able to distinguish between compounds transported by Oct1 from those that were not, we proceeded towards a more detailed determination of Oct1 interactions. We used oxaliplatin as the model cytotoxic zebrafish Oct1 substrate and investigated the effect of co-exposure of increasing concentrations of oxaliplatin with a single concentration of cisplatin, MPP+ or progesterone. We determined that MPP+ and progesterone abolished the effect of Oct1 overexpression to oxaliplatin cytotoxicity, whereas cisplatine did not show any modulation of cytotoxicity in the Oct1 overexpression cells in comparison to mock-transfected cells (Fig. 6).

4. Discussion

This study represents the first functional characterization of a fish organic cation transporter. Our primary goals were to elucidate the interaction of Oct1 with xenobiotics and endogenous compounds and, using a zebrafish model, offer initial insight into the potential role of Oct1 in the toxicological response of fish. As shown previously, zebrafish Oct1 was highly expressed in the kidney and liver, toxicologically important tissues, which indicated that Oct1, as a direct ortholog of human OCTs, may be an important element of the ADME processes in zebrafish (Mihaljevic et al., 2016). To functionally characterize zebrafish Oct1, we developed an *in vitro* assay with stably transfected cells and fluorescent dyes as model substrates. Five Oct1 fluorescent substrates were identified: ASP+, Rh123, berberine, DAPI and EtBr. ASP+ showed better kinetic parameters in comparison to other dyes, specifically showing a high transport velocity by zebrafish Oct1.

The observed differences in the Oct1-mediated transport of five different fluorescent substrates were probably caused by the presence of a high and low affinity binding site within the Oct1 active region, as suggested by Koepsell for rat Oct1 (2015). Zebrafish Oct1 showed high affinity for Rh123, DAPI and EtBr, whereas their maximum transport velocity values (V_{max}) were low (Table 1). Compared to the high affinity transport of these three substrates, ASP+ and berberine showed lower interaction affinity with Oct1, whereas their V_{max} values were considerably high (Table 1). Therefore, the complexity of the OCT/Oct active region, reported previously in human and other investigated mammalian species, is most probably present and relevant with respect to the transport properties of zebrafish Oct1. There is 42–53% of amino acid identity among vertebrate OCTs/Octs (Mihaljevic et al., 2016), and our homology modeling based on known structure of the bacterial MFS member lactose permease (LacY) revealed a high structural similarity with mammalian Oct1 orthologs (Koepsell, 2015). Structural analysis confirmed transmembrane topology of Oct1 with 12 TMDs, as well as the presence of characteristic large extracellular and intracellular loops (Fig. 1). Eight crucial amino acid residues (Trp219, Tyr223, Thr227, Arg440, Ile443, Phe447, Gln448 and Asp475), located in the TMDs of the zebrafish Oct1 active region, were previously shown to change the substrate affinities and transport rates of rat Oct1 (Gorboulev et al., 1999, 2005; Popp et al., 2005; Volk et al., 2009). These amino acid residues are conserved in humans as well as in zebrafish (Fig. 1, Fig. S3) and probably play important roles in the interaction between a substrate and the substrate-binding region (Koepsell, 2011). Our structural analysis of Oct1 also confirmed that these crucial amino acid residues were situated within the substrate-binding region inside the same TMDs as in mammalian orthologs (Fig. 1, Fig. S3).

Taking into account the structural similarities between zebrafish Oct1 and human orthologs, we pursued the functional characterization further using transport activity experiments with previously identified interactors of human OCTs. Prior to the interaction screening, we confirmed the expression and localization of Oct1 in the plasma membrane of HEK293T cells used as a heterologous expression system in our study (Fig. 2). The determined

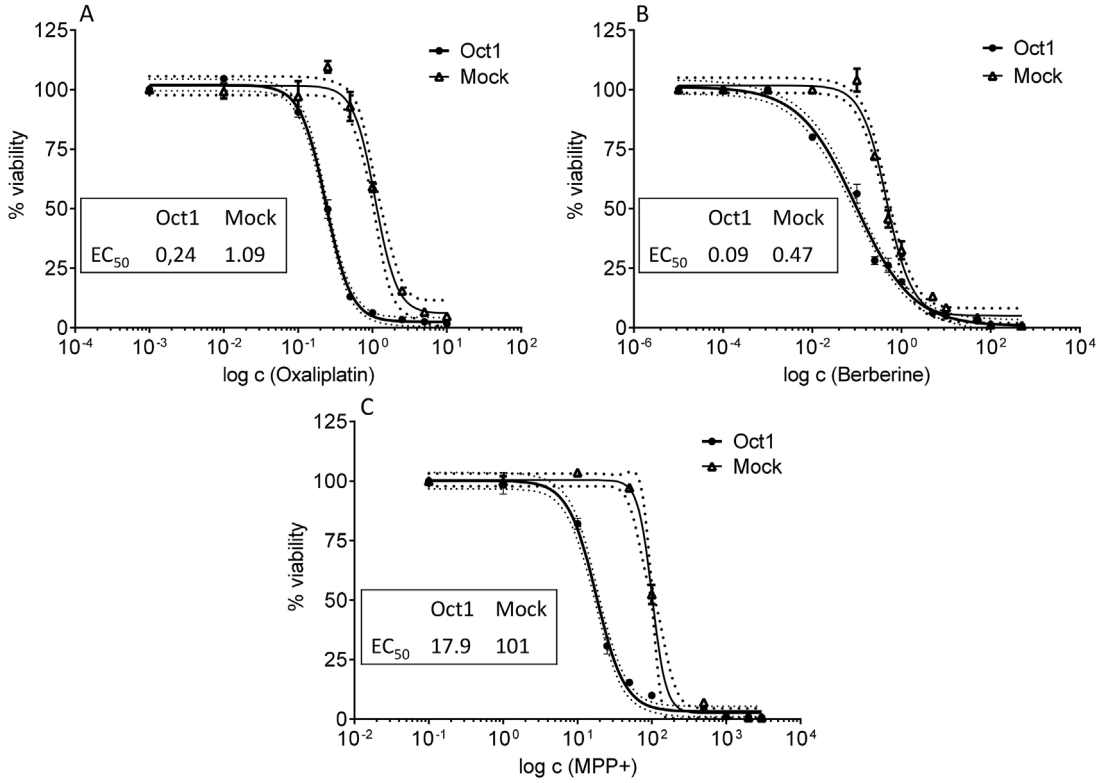

Fig. 4. Modulation of oxaliplatin (A), berberine (B) and MPP+ cytotoxicity (C) due to the overexpression of the zebrafish Oct1 in FlpIn/HEK293 cells, as determined using the MTT assay. The modulation is seen as a shift of the concentration-response curve to the left (lower EC_{50} in comparison with the mock-transfected cells). For the purpose of EC_{50} calculations, data were fitted to the sigmoidal four-parameter dose-response model (variable slope) in GraphPad Prism version 6. Each data point represents the mean ± S.E. from triplicate determinations.

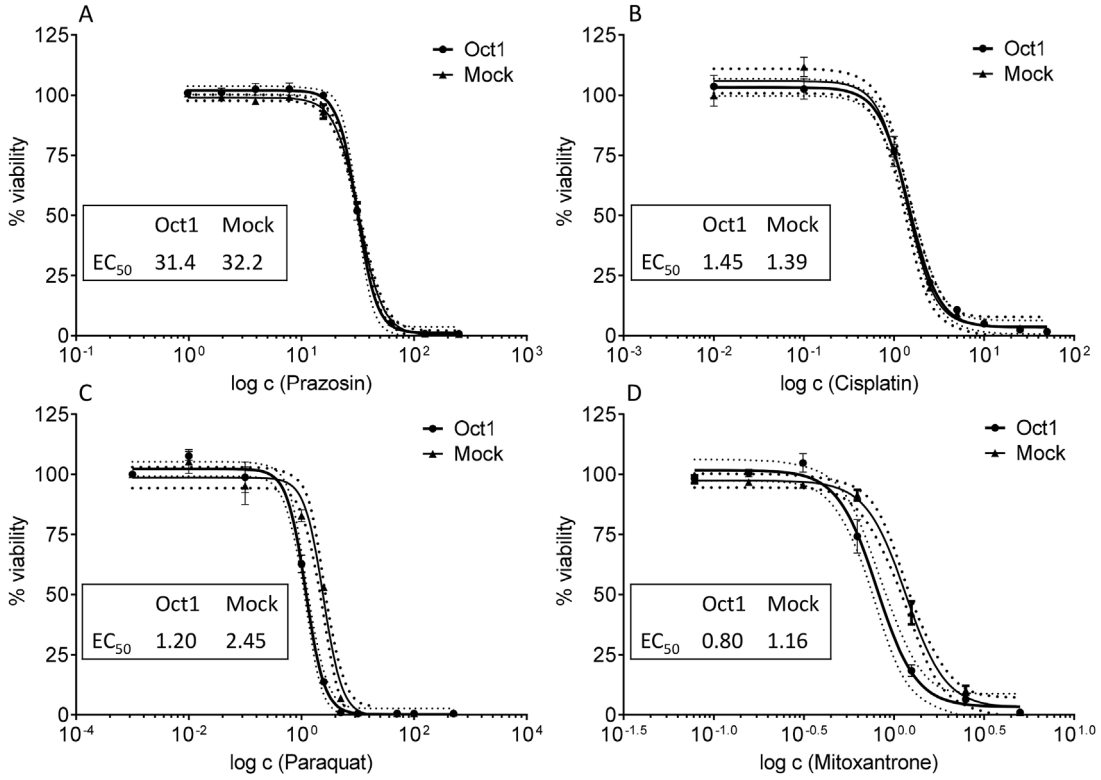

Fig. 5. Uncompetitive inhibitors prazosin (A), cisplatin (B), paraquat (C), and mitoxantrone (D) do not modulate cytotoxicity in FlpIn/HEK293 cells overexpressing zebrafish Oct1. For the purpose of EC_{50} calculations, data were fitted to the sigmoidal four-parameter dose-response model (variable slope) in GraphPad Prism version 6. Each data point represents the mean ± S.E. from triplicate determinations.

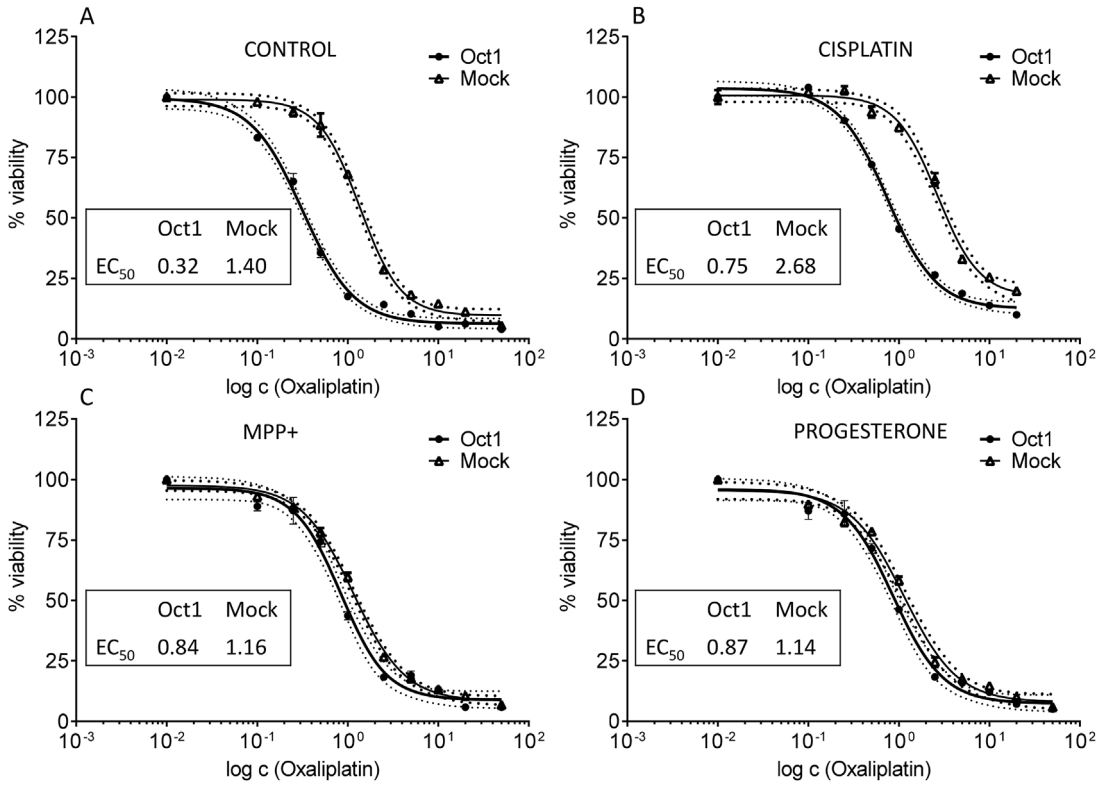

Fig. 6. Modulation of oxaliplatin cytotoxicity in the Oct1 overexpressing and mock-transfected cells exposed to increasing concentrations of oxaliplatin without or in the presence of single concentration of inhibitors transported by Oct1 or those that were not transported. (A) cytotoxicity of oxaliplatin in the Oct1 overexpressing and mock-transfected cells, without the inhibitors added (CONTROL); (B) co-exposure with cisplatin (0.5 μM); (C) co-exposure with MPP+ (1 μM); (D) co-exposure with progesterone (4 μM). For the purpose of EC_{50} calculations, data were fitted to the sigmoidal four-parameter dose-response model (variable slope) in GraphPad Prism version 6. Each data point represents the mean ± S.E. from triplicate determinations.

uptake preferences and basic kinetic parameters of the identified fluorescent substrates were then used as the basis for an interaction analysis of a wide range of potential Oct1 substrates and inhibitors that had not been transported. Zebrafish Oct1 showed interaction with known endogenous substrates of human and rodent OCTs/Octs (Nies et al., 2011). The IC_{50} values in the low millimolar range were determined for acetylcholine (711 μM) and tyramine (1002 μM). The acetylcholine IC_{50} value was similar to that reported for human OCT1, whereas tyramine showed a 5-fold lower IC_{50} value in interaction with human OCT1 (Bednarczyk et al., 2003; Lips et al., 2005). Additionally, acetylcholine revealed similarity between zebrafish Oct1 and human OCT1, whereas human OCT2 showed a high transport affinity of acetylcholine with a K_m value of 117 μM. OCT2-specific transport was also reported for choline, dopamine, creatinine and N1-methylnicotinamide. Histamine, norepinephrine, epinephrine, and the neuromodulators histidyl-proline diketopiperazine (cyclo(His-Pro)) and salsolinol, together with the L-arginine metabolite agmatine were transported by all three human orthologs (Nies et al., 2011; Koepsell, 2013; Boxberger et al., 2014; Chen et al., 2014; Müller et al., 2015). Strong interactions were determined with steroid hormones. By comparing the IC_{50} values of human and zebrafish OCT/Oct, zebrafish Oct1 was found to be similar to human OCT1 and OCT2 orthologs: progesterone and testosterone inhibited zebrafish Oct1-mediated transport with similar IC_{50} values as human OCT1, IC_{50} for β-estradiol was similar to human OCT2, while corticosterone IC_{50} was similar to both human OCT1 and OCT2 (Zhang et al., 1998; Hayer-Zillgen et al., 2002; Nies et al., 2011).

To assess the potential role of zebrafish Oct1 in cellular defense and ADME processes, we extended our interaction studies to several groups of xenobiotics. Our selection was based on their reported interactions with human or mammalian OCTs/Octs and/or their cationic nature. The interaction of zebrafish Oct1 with TEA (IC_{50} = 821 μM) was similar to the interaction reported for human OCT1 (IC_{50} = 158–1390 μM), whereas OCT2 and OCT3 showed both lower and higher IC_{50} values, respectively (Dresser et al., 2002; Kimura et al., 2009; Ming et al., 2009).

Other model cations from the group of tertiary ammonium ions, TBA and TPenA, showed overlapping IC_{50} values for zebrafish Oct1 transport, which is similar to the interaction pattern and range reported for human OCTs (Gorboulev et al., 1997; Zhang et al., 1998; Dresser et al., 2002). A similar effect was obtained with another model cation, MPP+, with a similar IC_{50} value to those of human OCT1 and OCT2 (Gorboulev et al., 1997; Gründemann et al., 2003). The most potent xenobiotic interactors of Oct1 were organotin chlorides, a group of highly deleterious environmental contaminants (Fent, 1996). Our study is the first report of an interaction of organotin chlorides with organic cation transporters, with the most potent effect determined for dibutyltin chloride, followed by tributyltin and tripropyltin chloride (Table 2). Regardless of the regulation of organotin compound usage in some countries due to their harmful effects on aquatic environments, high concentrations of TBT are nevertheless found in such environments, with nanomolar concentrations found in fish, suggesting a potentially important role for fish Oct1 in the toxicological response in organotin-contaminated aquatic environments (Hotch, 2001).

A potent interaction of zebrafish Oct1 was obtained for the antimalarial drug pyrimethamine, whose IC_{50} value of 0.4 μM was almost 10 and 25 times lower than values reported for human OCT1 and OCT2, respectively (Ito et al., 2010). The sympatholytic drug prazosin inhibited Oct1-mediated transport with similar affinity as human OCT1 (Minematsu et al., 2010). The reported IC_{50}

value of the antiarrhythmic drug verapamil was similar to the reported value for human OCT2 (Minematsu et al., 2010), whereas the interaction of Oct1 with the other investigated antiarrhythmics, propranolol and quinidine, was more similar to human OCT1 (Zhang et al., 1998; Ahlin et al., 2008). Interestingly, a rare similarity related to human OCT3 interaction strengths was determined for the antidepressant imipramine and antihypertensive diltiazem (Wu et al., 2000; Umehara et al., 2008). Investigation on the effect of antineoplastic drugs on zebrafish Oct1 activity revealed mitoxantrone as the most potent drug, similarly to human OCT1, whereas tamoxifen showed similarity to human OCT2. The cisplatin and oxaliplatin Oct1 interaction pattern was similar to interactions previously reported with human orthologs, with cisplatin showing a more potent interaction with OCT2 than oxaliplatin (Ciarimboli et al., 2005; Yonezawa et al., 2006). Vandetanib and dasatinib, representing another group of antineoplastic drugs from the class of tyrosine kinase inhibitors (TKIs), showed a potent inhibition of zebrafish Oct1 transport which is in correlation with findings that demonstrated an effect of TKIs on the post-translational regulation of human OCT2 (Sprowl et al., 2016).

Based on the described identification of xenobiotic Oct1 interactors, in the final part of our study we obtained the first indications regarding the possible role of Oct1 in the zebrafish toxicological response. Using our expression system, we also aimed at determining the type of interaction of the investigated compounds with zebrafish Oct1, discerning between Oct1-transported substrates and inhibitors that had not been transported. The initial cytotoxicity tests performed using the MTT assay revealed that MPP+, as an Oct1 substrate, caused the Oct1-overexpressing cells to be more susceptible to the toxic effect of this known neurotoxin (Wiemerslage and Lee, 2016) in comparison to mock-transfected cells. MPP+ showed an EC_{50} value of 18.0 μM which was similar to its determined IC_{50} value of 22.3 μM (Table 2, Fig. 4). Likewise, Oct1-overexpressing cells exhibited much higher sensitivity to the other two identified substrates, berberine and oxaliplatin, with EC_{50} values of 95.7 nM and 236 nm, respectively (Fig. 4).

Furthermore, a comparison of the determined Oct1 interaction strengths (IC_{50} values) and toxic potencies (EC_{50} values) revealed that the identified interactors may have toxic effects in zebrafish even at concentrations below the determined IC_{50} values. Therefore, due to the already frequent and still growing usage of oxaliplatin as a neoplastic drug, and berberine as an antidiabetic and anticancer drug with unclear outcomes in the environment, the determined EC_{50} values point to their potential environmental relevance (Besse et al., 2012; Liu et al., 2016). It is also important to note that the harmful effects of the identified toxic Oct1 substrates may occur indirectly, through Oct1-mediated uptake through the intestine and potentially gills, elevating the concentration of potential toxins in plasma. In addition, the inhibition of Oct1 primarily expressed in zebrafish kidneys could destabilize the excretion of deleterious compounds, which may in turn lead to toxic effect of other, normally non-toxic xenobiotics or endogenous compounds (Hagos et al., 2016). Finally, using our test system we showed that MPP+ and progesterone were able to completely abolish the elevated cytotoxicity of oxaliplatin in Oct1-overexpressing cells (Fig. 6). The observed effects confirmed that these compounds are indeed competitive inhibitors (i.e. substrates) of zebrafish Oct1, whereas cisplatin proved to be an Oct1 inhibitor that is not transported (Fig. 6).

In conclusion, this study provides a structural model of zebrafish Oct1 which revealed similarities and differences with human and mammalian orthologs, with special emphasis on the complexity of the OCT/Oct active region. The presented structural model can be used for a more detailed investigation of zebrafish Oct1 and the characterization of its active region. Our interaction tests showed the polyspecific nature of zebrafish Oct1. Altogether, the high expression of zebrafish Oct1 in the liver and kidney, in addition to the high number of diverse endo- and xenobiotic interactors, suggested a similar function of zebrafish Oct1 to both human OCT1 and OCT2. Finally, our experiments on the cytotoxicity modulation of model Oct1 substrates pinpointed four transported substrates – progesterone as a physiologically relevant substrate, and oxaliplatin, berberine and MPP+ as environmentally relevant and potentially toxic Oct1 substrates – providing bases for further *in vivo* studies needed for the evaluation of the ecotoxicological relevance of this membrane transport protein in fish.

Acknowledgements

This research was supported by the Croatian National Science Foundation (Project No. 4806) and SCOPES joint research project supported by the Swiss National Science Foundation (SNSF) (Grant No. SCOPES – IZ73ZO_152274/1).

Appendix A. Supplementary data

Supplementary data associated with this article can be found, in the online version, at http://dx.doi.org/10.1016/j.aquatox.2017.03.012.

References

Abramson, J., Smirnova, I., Kasho, V., Verner, G., Kaback, H.R., Iwata, S., 2003. Structure and mechanism of the lactose permease of Escherichia coli. Science 301, 610–615.

Ahlin, G., Karlsson, J., Pedersen, J.M., Gustavsson, L., Larsson, R., Matsson, P., Norinder, U., Bergström, C.A., Artursson, P., 2008. Structural requirements for drug inhibition of the liver specific human organic cation transport protein 1. J. Med. Chem. 51, 5932–5942.

Bednarczyk, D., Ekins, S., Wikel, J.H., Wright, S.H., 2003. Influence of molecular structure on substrate binding to the human organic cation transporter, hOCT1. Mol. Pharmacol. 63, 489–498.

Besse, J.-P., Latour, J.-F., Garric, J., 2012. Anticancer drugs in surface waters: what can we say about the occurrence and environmental significance of cytotoxic, cytostatic and endocrine therapy drugs? Environ. Int. 39, 73–86.

Boxberger, K.H., Hagenbuch, B., Lampe, J.N., 2014. Common drugs inhibit human organic cation transporter 1 (OCT1)-mediated neurotransmitter uptake. Drug Metab. Dispos. 42, 990–995.

Brast, S., Grabner, A., Sucic, S., Sitte, H.H., Hermann, E., Pavenstädt, H., Schlatter, E., Ciarimboli, G., 2012. The cysteines of the extracellular loop are crucial for trafficking of human organic cation transporter 2 to the plasma membrane and are involved in oligomerization. FASEB J. 26, 976–986.

Bradford, M.M., 1976. A rapid and sensitive method for the quantitation of microgram quantities of protein utilizing the principle of protein-dye binding. Anal. Biochem. 72, 248–254.

Busch, A.E., Quester, S., Ulzheimer, J.C., Gorboulev, V., Akhoundova, A., Waldegger, S., Lang, F., Koepsell, H., 1996. Monoamine neurotransmitter transport mediated by the polyspecific cation transporter rOCT1. FEBS Lett. 395, 153–156.

Chen, J.J., Li, Z., Pan, H., Murphy, D.L., Tamir, H., Koepsell, H., Gershon, M., 2001. Maintenance of serotonin in the intestinal mucosa and ganglia of mice that lack the high-affinity serotonin transporter: abnormal intestinal motility and the expression of cation transporters. J. Neurosci. 21, 6348–6361.

Chen, L., Shu, Y., Liang, X., Chen, E.C., Yee, S.W., Zur, A.A., Li, S., Xu, L., Keshari, K.R., Lin, M.J., Chien, H.-C., Zhang, Y., Morrissey, K.M., Liu, J., Ostrem, J., Younger, N.S., Kurhanewicz, J., Shokat, K.M., Ashrafi, K., Giacomini, K.M., 2014. OCT1 is a high-capacity thiamine transporter that regulates hepatic steatosis and is a target of metformin. Proc. Natl. Acad. Sci. U. S. A. 111, 9983–9988.

Ciarimboli, G., Ludwig, T., Lang, D., Pavenstädt, H., Koepsell, H., Piechota, H.J., Haier, J., Jaehde, U., Zisowsky, J., Schlatter, E., 2005. Cisplatin nephrotoxicity is critically mediated via the human organic cation transporter 2. Am. J. Pathol. 167, 1477–1484.

Dresser, M.J., Xiao, G., Leabman, M.K., Gray, A.T., Giacomini, K.M., 2002. Interactions of n-tetraalkylammonium compounds and biguanides with a human renal organic cation transporter (hOCT2). Pharm. Res. 19, 1244–1247.

Fent, K., 1996. Ecotoxicology of organotin compounds. CRC Crit. Rev. Toxicol. 26, 1–117.

Gorboulev, V., Ulzheimer, J.C., Akhoundova, A., Ulzheimer-Teuber, I., Karbach, U., Quester, S., Baumann, C., Lang, F., Busch, A.E., Koepsell, H., 1997. Cloning and characterization of two human polyspecific organic cation transporters. DNA Cell Biol. 16, 871–881.

Gorboulev, V., Volk, C., Arndt, P., Akhoundova, A., Koepsell, H., 1999. Selectivity of the polyspecific cation transporter rOCT1 is changed by mutation of aspartate 475 to glutamate. Mol. Pharmacol. 56, 1254–1261.

Gorboulev, V., Shatskaya, N., Volk, C., Koepsell, H., 2005. Subtype-specific affinity for corticosterone of rat organic cation transporters rOCT1 and rOCT2 depends on three amino acids within the substrate binding region. Mol. Pharmacol. 67, 1612–1619.
Gründemann, D., Hahne, C., Berkels, R., Schömig, E., 2003. Agmatine is efficiently transported by non-neuronal monoamine transporters extraneuronal monoamine transporter (EMT) and organic cation transporter 2 (OCT2). J. Pharmacol. Exp. Therap. 304, 810–817.
Hagos, F.T., Daood, M.J., Ocque, J.A., Nolin, T.D., Bayir, H., Poloyac, S.M., Kochanek, P.M., Clark, R.S., Empey, P.E., 2016. Probenecid, an organic anion transporter 1 and 3 inhibitor: increases plasma and brain exposure of N-acetylcysteine. Xenobiotica 9, 1–8.
Hayer-Zillgen, M., Brüss, M., Bönisch, H., 2002. Expression and pharmacological profile of the human organic cation transporters hOCT1 hOCT2 and hOCT3. Br. J. Pharmacol. 136, 829–836.
Hendrickx, R., Johansson, J.G., Lohmann, C., Jenvert, R.M., Blomgren, A., Börjesson, L., Gustavsson, L., 2013. Identification of novel substrates and structure activity relationship of cellular uptake mediated by the human organic cation transporters 1 and 2 (hOCT1 and hOCT2). J. Med. Chem. 56, 7232–7242.
Hotch, M., 2001. Organotin compounds in the environment –an overview. Appl. Geochem. 16, 719–743.
Inazu, M., Takeda, H., Matsumiya, T., 2003. Expression and functional characterization of the extraneuronal monoamine transporter in normal human astrocytes. J. Neurochem. 84, 43–52.
Ito, S., Kusuhara, H., Kuroiwa, Y., Wu, C., Moriyama, Y., Inoue, K., Kondo, T., Yuasa, H., Nakayama, H., Horita, S., Sugiyama, Y., 2010. Potent and specific inhibition of mmate1-mediated efflux of type I organic cations in the liver and kidney by pyrimethamine. J. Pharmacol. Exp. Therap. 333, 341–350.
Keller, T., Egenberger, B., Gorboulev, V., Bernhard, F., Uzelac, Z., Gorbunov, D., Wirth, C., Koppatz, S., Dötsch, V., Hunte, C., Sitte, H.H., Koepsell, H., 2011. The large extracellular loop of organic cation transporter 1 influences substrate affinity and is pivotal for oligomerization. J. Biol. Chem. 286, 37874–37884.
Kimura, N., Masuda, S., Katsura, T., Inui, K., 2009. Transport of guanidine compounds by human organic cation transporters, hOCT1 and hOCT2. Biochem. Pharmacol. 77, 1429–1436.
Koepsell, H., Schmitt, B., M Gorboulev, V., 2003. Organic cation transporters. Rev. Physiol. Biochem. Pharmacol. 150, 36–90.
Koepsell, H., 2011. Substrate recognition and translocation by polyspecific organic cation transporters. Biol. Chem. 392, 95–101.
Koepsell, H., 2013. The SLC22 family with transporters of organic cations, anions and zwitterions. Mol. Aspects Med. 34, 413–435.
Koepsell, H., 2015. Role of organic cation transporters in drug—drug interaction. Expert Opin. Drug Metab. Toxicol. 11, 1619–1633.
Lips, K.S., Volk, C., Schmitt, B.M., Pfeil, U., Arndt, P., Miska, D., Ermert, L., Kummer, W., Koepsell, H., 2005. Polyspecific cation transporters mediate luminal release of acetylcholine from bronchial epithelium. Am. J. Respir. Cell Mol. Biol. 33, 79–88.
Liu, C.-S., Zheng, Y.-R., Zhang, Y.-F., Long, X.-Y., 2016. Research progress on berberine with a special focus on its oral bioavailability. Fitoterapia 109, 274–282.
Müller, F., Pontones, C.A., Renner, B., Mieth, M., Hoier, E., Auge, D., Maas, R., Zolk, O., Fromm, M.F., 2015. N1-methylnicotinamide as an endogenous probe for drug interactions by renal cation transporters: studies on the metformin–trimethoprim interaction. Eur. J. Clin. Pharmacol. 71, 85–94.
Mihaljevic, I., Popovic, M., Zaja, R., Smital, T., 2016. Phylogenetic, syntenic, and tissue expression analysis of slc22 genes in zebrafish (Danio rerio). BMC Genomics. 17, 626–639.
Minematsu, T., Iwai, M., Umehara, K., Usui, T., Kamimura, H., 2010. Characterization of human organic cation transporter 1 (OCT1/SLC22A1)- and OCT2 (SLC22A2)-mediated transport of 1-(2-methoxyethyl) 2-methyl-4, 9-dioxo-3-(pyrazin-2-ylmethyl)- 4, 9-dihydro-1H-naphtho[2, 3-d]imidazolium bromide (YM155 monobromide), a novel small molecule survivin suppressant. Drug Metab. Dispos. 38, 1–4.
Ming, X., Ju, W., Wu, H., Tidwell, R.R., Hall, J.E., Thakker, D.R., 2009. Transport of dicationic drugs pentamidine and furamidine by human organic cation transporters. Drug Metab. Dispos. 37, 424–430.
Mosmann, T., 1983. Rapid colorimetric assay for cellular growth and survival: application to proliferation and cytotoxicity assays. J. Immunol. Meth. 65, 55–63.
Motohashi, H., Sakurai, Y., Saito, H., Masuda, S., Urakami, Y., Goto, M., Fukatsu, A., Ogawa, O., Inui, K., 2002. Gene expression levels and immunolocalization of organic ion transporters in the human kidney. J. Am. Soc. Nephrol. 13, 866–874.
Nies, A.T., Koepsell, H., Damme, K., Schwab, M., 2011. Organic cation transporters (OCTs, MATEs), in vitro and in vivo evidence for the importance in drug therapy. In: Fromm, M.F., Kim, R.B. (Eds.), Drug Transporters, Handbook of Experimental Pharmacology 201. Springer-Verlag Berlin Heidelberg, pp. 105–167.
Popovic, M., Zaja, R., Fent, K., Smital, T., 2013. Molecular characterization of zebrafish Oatp1d1 (Slco1d1), a novel organic anion-transporting polypeptide. J. Biol. Chem. 22, 33894–33911.
Popp, C., Gorboulev, V., Müller, T.D., Gorbunov, D., Shatskaya, N., Koepsell, H., 2005. Amino acids critical for substrate affinity of rat organic cation transporter 1 line the substrate binding region in a model derived from the tertiary structure of lactose permease. Mol. Pharmacol. 67, 1600–1611.
Sali, A., Blundell, T.L., 1993. Comparative protein modeling by satisfaction of spatial restraints. Mol. Biol. 234, 779–815.
Sambrook, J.F., Fritsch, E.F., Maniatis, T., 1989. Molecular Cloning – A Laboratory Manual. Cold Spring Harbor Laboratory Press Cold Spring Harbor, NY, USA.
Schlatter, E., Klassen, P., Massmann, V., Holle, S.K., Guckel, D., Edemir, B., Pavenstädt, H., Ciarimboli, G., 2014. Mouse organic cation transporter 1 determines properties and regulation of basolateral organic cation transport in renal proximal tubules. Eur. J. Physiol. 466, 1581–1589.
Shen, M.Y., Sali, A., 2006. Statistical potential for assessment and prediction of protein structures. Protein Sci. 15, 2507–2524.
Sprowl, J.A., Ong, S.S., Gibson, A.A., Hu, S., Du, G., Lin, W., Li, L., Bharill, S., Ness, R.A., Stecula, A., Offer, S.M., Diasio, R.B., Nies, A.T., Schwab, M., Cavaletti, G., Schlatter, E., Ciarimboli, G., Schellens, J.H., Isacoff, E.Y., Sali, A., Chen, T., Baker, S.D., Sparreboom, A., Pabla, N., 2016. A phosphotyrosine switch regulates organic cation transporters. Nat. Commun. 7, 10880.
Sweet, D.H., Miller, D.S., Pritchard, J.B., 2001. Ventricular choline transport. J. Biol. Chem. 276, 41611–41619.
Umehara, K.I., Iwatsubo, T., Noguchi, K., Usui, T., Kamimura, H., 2008. Effect of cationic drugs on the transporting activity of human and rat OCT/Oct 1–3 in vitro and implications for drug–drug interactions. Xenobiotica 38, 1203–1218.
Volk, C., Gorboulev, V., Kotzsch, A., Müller, T.D., Koepsell, H., 2009. Five amino acids in the innermost cavity of the substrate binding cleft of organic cation transporter 1 interact with extracellular and intracellular corticosterone. Mol. Pharmacol. 76, 275–289.
Wiemerslage, L., Lee, D., 2016. Quantification of mitochondrial morphology in neurites of dopaminergic neurons using multiple parameters. J. Neurosci. Methods 262, 56–65.
Wu, X., Huang, W., Ganapathy, M.E., Wang, H., Kekuda, R., Conway, S.J., Leibach, F.H., Ganapathy, V., 2000. Structure, function, and regional distribution of the organic cation transporter OCT3 in the kidney. Am. J. Physiol. Renal Physiol. 279, 449–458.
Yonezawa, A., Masuda, S., Yokoo, S., Katsura, T., Inui, K., 2006. Cisplatin and oxaliplatin, but not carboplatin and nedaplatin, are substrates for human organic cation transporters (SLC22A1-3 and multidrug and toxin extrusion family). J. Pharmacol. Exp. Therap. 319, 879–886.
Zhang, L., Schaner, M.E., Giacomini, K.M., 1998. Functional characterization of an organic cation transporter (hOCT1) in a transiently transfected human cell line (HeLa). J. Pharmacol. Exp. Therap. 286, 354–361.
Zhang, T., Xiang, C.D., Gale, D., Carreiro, S., Wu, E.Y., Zhang, E.Y., 2008. Drug transporter and cytochrome P450 mRNA expression in human ocular barriers: implications for ocular drug disposition. Drug Metab. Dispos. 36, 1300–1307.
Zhu, C., Nigam, K.B., Date, R.C., Bush, K.T., Springer, S.A., Saier Jr., M.H., Wu, W., Nigam, S.K., 2015. Evolutionary analysis and classification of OATs, OCTs, OCTNs, and other SLC22 transporters: structure-function implications and analysis of sequence motifs. PLoS One 10 (11), e0140569.